ATOM PHYSICS AND PHYSICS OF CLUSTERS AND NANOSTRUCTURES

Original article
DOI: https://doi.org/10.18721/JPM.16203

THE PLASMON RESONANCE IN THE CADMIUM SELENIDE SEMICONDUCTOR NANOCRYSTALS WITH DIFFERENT DOPING TYPES

A. N. Ipatov[1, 2], *G. A. Kupriianov*[1]✉

[1] Peter the Great St. Petersburg Polytechnic University, St. Petersburg, Russia;

[2] Alferov University of RAS, St. Petersburg, Russia

✉ henryweis3@gmail.com

Abstract. The effect of the type of doping (surface (I) or bulk (II) doping) on the character of the dipole plasmon mode in semiconductor CdSe nanocrystals has been studied. It was found that in case I (donors located on the surface of the nanocrystal) the collective mode had a rotational character and only the angular degrees of freedom were excited. On the contrary, in case II the charge of the dopant impurities was distributed throughout the system and plasmon excitation was the oscillation of delocalized charge carriers in the direction normal to the surface. It was shown that the position of the resonance line was determined not only by the concentration of free charges, but also by the character of their collective motion determining by the type of doping.

Keywords: semiconductor nanocrystal, cadmium selenide, doping, plasmon resonance, multiparticle excitation

Citation: Ipatov A. N., Kupriianov G. A., The plasmon resonance in the cadmium selenide semiconductor nanocrystals with different doping types, St. Petersburg State Polytechnical University Journal. Physics and Mathematics. 16 (2) (2023) 27–51. DOI: https://doi.org/10.18721/JPM.16203

Научная статья
УДК 538.9
DOI: https://doi.org/10.18721/JPM.16203

ПЛАЗМОННЫЙ РЕЗОНАНС В ПОЛУПРОВОДНИКОВЫХ НАНОКРИСТАЛЛАХ СЕЛЕНИДА КАДМИЯ С РАЗЛИЧНЫМ ТИПОМ ЛЕГИРОВАНИЯ

А. Н. Ипатов[1, 2], *Г. А. Куприянов*[1] ✉

[1] Санкт-Петербургский политехнический университет Петра Великого, Санкт-Петербург, Россия;

[2] Академический университет им. Ж.И. Алфёрова РАН, Санкт-Петербург, Россия

✉ henryweis3@gmail.com

Аннотация. Исследовано влияние типа легирования (поверхностное (I) либо объемное (II)) на характер дипольной плазмонной моды в полупроводниковых нанокристаллах CdSe. Установлено, что в I случае (доноры расположены на поверхности нанокристалла) коллективная мода имеет вращательный характер и возбуждаются только угловые степени свободы. Напротив, во II случае заряд легирующих примесей распределен по всему объему системы и плазмонное возбуждение – суть колебание делокализованных носителей заряда в направлении нормали к поверхности. Показано, что положение резонансной линии обусловлено не только концентрацией свободных зарядов, но и характером их коллективного движения, который определяется типом легирования.

Ключевые слова: полупроводниковый нанокристалл, селенид кадмия, легирование, плазмонный резонанс, многочастичное возбуждение

Ссылка для цитирования: Ипатов А. Н., Куприянов Г. А. Плазмонный резонанс в полупроводниковых нанокристаллах селенида кадмия с различным типом легирования // Научно-технические ведомости СПбГПУ. Физико-математические науки. 2023. Т. 16. № 2. С. 27–51. DOI: https://doi.org/10.18721/ JPM.16203

Introduction

Recent decades have seen rapid advances in nanotechnology, nanoelectronics and nanophotonics, with the pressing need for novel materials whose physical and chemical properties differ from those of the corresponding bulk components. A burgeoning field is quantum plasmonics focused on studying the quantum properties of light and the mechanisms of its interaction with matter at the nanoscale level [1–3]. A distinct characteristic of nanoscale conducting particles is the presence of dipole resonances in their optical spectra [2, 4–8]. In particular, doped semiconductor nanocrystals are a promising class of materials [4, 5, 9–15]. Importantly, the position of the resonance line in the spectra of semiconductor nanoparticles depends not only on the concentration of carriers, but also on the doping method, which can be provisionally defined as either bulk or surface [16–20]. In the first case, the charge density of free carriers is distributed over the entire volume of the crystal and is at the same time neutralized by the charge of dopant impurities, while in the second case, free carriers are injected into the bulk of the semiconductor nanoparticle by donors/acceptors located on its surface [21, 22]. In the case of bulk-doped semiconductor nanoparticles [18–20, 23], a dipole plasmon can be described in the adiabatic approximation [24, 25] as a quasi-particle making harmonic oscillations of a system of delocalized electrons as a whole relative to the center of the positively charged core in the direction normal to its surface.

On the other hand, it was established in [26, 27] that the situation turns out to be fundamentally different for surface-doped nanocrystals. The characteristics of the electronic configuration induced by the surface doping mechanism generate excitation states of only angular degrees of freedom in the collective dipole mode upon interaction with an external electromagnetic field. The motion of electrons in the radial direction is not included, and the electrons oscillate tangentially with respect to the boundary of the system within a relatively thin spherical layer. The described phenomenon is similar to dipole plasmon oscillations in fullerenes [28–30].

The goal of the study was to detect and analyze the influence of the doping type, the number of delocalized charge carriers, as well as the geometric dimensions of the system on the nature of multiparticle excitations in the electron system of doped semiconductor nanocrystals, focusing on cadmium selenide CdSe nanocrystals.

Our approach to analysis of the phenomenon is based on a self-consistent quantum mechanical description of multiparticle excitations in a system of delocalized charge carriers. Calculations of the system's ground state were carried out in the Hartree–Fock approximation, taking into account the nonlocal interparticle exchange interaction. For comparison, the calculations were complemented by calculations performed in the local density approximation; the photoabsorption spectra of nanocrystals containing a different number of free charge carriers were obtained within the random phase approximation (RPA) both with nonlocal (RPAE) and local (RPAX) exchange interactions [31, 32].

Theoretical approach

We examine *n*-doped CdSe nanocrystals in a dielectric environment with different types of doping, as, according to the approach to the problem outlined in [19, 20], it determines the form of effective external potential where delocalized charge carriers move, and, accordingly, their distribution across the bulk of the nanocrystal.

Consider an electroneutral system of interacting fermions related by the Coulomb interaction. Negative particles in the conduction band are referred to as electrons with an effective mass m_e from now on.

The total Hamiltonian of the described system is an operator of the total energy of a system of N electrons interacting with each other by means of the Coulomb potential V in the external potential $U_{ext}(\mathbf{r})$, whose radial dependence is determined by the doping type:

$$\hat{H} = \sum_{i}^{N} \frac{\hat{\mathbf{p}}_i}{2m_e} + \sum_{i}^{N} U_{ext}(r_i) + \frac{1}{2}\sum_{i,j}^{N} V(\mathbf{r}_i, \mathbf{r'}_j). \tag{1}$$

Since the motion of electrons within the nanoparticle bulk is limited by the edge of the conduction band near the surface [13], we describe $U_{ext}(\mathbf{r})$ as a spherical potential well, whose geometric parameter R is determined by the dimensions set for the nanocrystal and the profile by the selected type of doping. The Coulomb pair interaction between electrons at points $\mathbf{r}_a$ and $\mathbf{r}_b$ is shielded due to polarization of both the semiconductor material itself and the environment, so that the multipole expansion of the interparticle interaction potential at $r_i, r_j < R$ can be written as follows [33, 34]:

$$V(\mathbf{r}_i, \mathbf{r}_j) = \sum_{LM} \frac{V_L}{2L+1} Y_{LM}(\mathbf{r}_i) Y^*_{LM}(\mathbf{r}_j),$$
$$V_L = \frac{4\pi e^2}{\varepsilon_1}\left(\frac{r_<^L}{r_>^{L+1}} + \frac{(\varepsilon_1 - \varepsilon_2)(L+1)(r_i r_j)^L}{(L\varepsilon_1 + (L+1)\varepsilon_2)R^{2L+1}}\right), \tag{2}$$

where $r_{>,<}$ are the largest and the smallest of the radii $r_{i,j}$, respectively; ε_1, ε_2 are the permittivity of nanocrystal materials and its surrounding environment, respectively; L, M are the total angular momentum and its projection, respectively; Y_{LM}, Y^*_{LM} are complex conjugate spherical functions; $\mathbf{r}_i$, $\mathbf{r}_j$ are the radius vectors of interacting particles.

It was assumed in the numerical calculations that the dielectric constant of cadmium selenide is equal to its value for the corresponding bulk material: $\varepsilon_1 = 6.25$, and the permittivity of the nanoparticle environment was chosen typical for a number of experimental and theoretical works [19, 21, 22]: $\varepsilon_2 = 2.25$. For comparison with some conclusions drawn in [19], numerical calculations were carried out at a value of $R = 2$ nm.

Importantly, since the effective electron mass of the electrons in cadmium selenide is relatively small relative to the mass of the free electron, namely $m_e = 0.11\ m_0$, and the effective Bohr radius a_0 turns out to be larger than the radius of the considered nanoparticles R,

$$a_0 = h^2\varepsilon_1/m_e e^2 = 3 \text{ nm},$$

this is fundamentally different from the situation with ZnO nanocrystals whose optical properties were discussed in [21, 22, 26, 27].

The interparticle interaction in the ground state of the system was described using, the Hartree–Fock (HF) approximation where the single-particle wave functions of the electrons $\phi(\mathbf{r}_i)$ satisfy the self-consistent equations [35–37]:

$$-\frac{\hbar^2\Delta_i}{2m_e}\phi_i(\mathbf{r}_i) + \left(U_{ext}(\mathbf{r}_i) + U_H(\mathbf{r}_i) + U_x(\mathbf{r}_i)\right)\phi_i(\mathbf{r}_i) = E_i\phi_i(\mathbf{r}_i), \tag{3}$$

where E_i are single-particle electron energies, $U_H(\mathbf{r})$ is the corresponding Hartree potential.

In the case of a system with filled shells, they are written as [37]

$$U_H(\mathbf{r}) = \int V(\mathbf{r},\mathbf{r}')\rho_e(\mathbf{r}')d\mathbf{r}', \tag{4}$$

where the bulk electron density

$$\rho_e(\mathbf{r}) = 2\sum\nolimits_i \phi_i^*(\mathbf{r})\phi_i(\mathbf{r})$$

is calculated by summing over all filled single-particle states.

In this case, the contribution of the nonlocal exchange potential $U_x(\mathbf{r})$ is defined as

$$U_x(\mathbf{r})\phi_i(\mathbf{r}) = -e^2\sum_j \int \frac{\phi_j^*(\mathbf{r}')\phi_i(\mathbf{r}')d\mathbf{r}'}{|\mathbf{r}-\mathbf{r}'|}\phi_j(\mathbf{r}). \tag{5}$$

The computational results were compared with the corresponding values obtained in the local density approximation (LDA), implying that single-particle wave functions of electrons $\phi_i(\mathbf{r})$ satisfy the Kohn–Sham equations [38], where, unlike Eq. (3), local exchange potentials $U_x(\mathbf{r})$ are used in the Dirac–Slater approximation [38]:

$$U_x(\mathbf{r}) = -\left(e^2/\varepsilon_1\right)\left(3\rho_e(\mathbf{r})/\pi\right)^{1/3}. \tag{6}$$

In the case of spherically symmetric systems with closed electron shells and isotropic angular dependencies $\mathrm{p}(\mathbf{r})$ and $U_{ext}(\mathbf{r})$, the collective index i is equal to $i = (n,l,m,\sigma)$, where n is the radial quantum number; l, m are the orbital angular momentum and its projection; σ is the spin projection, while the actual single-particle wave functions are written as the product of the radial, angular and spin components [39]:

$$\phi_{nlm\sigma}(\mathbf{r}) = \frac{P_{nl}(r)}{r}Y_{lm}(\theta,\varphi)\chi_\sigma. \tag{7}$$

The random phase approximation with nonlocal exchange interaction was used to describe multielectron correlations. The wave function of the excited state $|\Phi_k\rangle$ is represented within this approach as a superposition of single-particle excitations of the particle–vacancy type:

$$\left|\Phi_k\right\rangle = \sum_{im}\left(X_{im}^{(k)}\hat{a}_m^+\hat{a}_i + Y_{im}^{(k)}\hat{a}_i^+\hat{a}_m\right)\left|\Phi_0\right\rangle, \tag{8}$$

where $|\Phi_0\rangle$ is the ground state of the complex; $\hat{a}^+$, $\hat{a}$ are single-particle operators of creation and annihilation; the indices i, m are used (here and below) to denote filled and unfilled single-particle states of the electronic subsystem; the coefficients $X_{im}^{(k)}$, $Y_{im}^{(k)}$ are the forward-in-time and backward-in-time amplitudes, respectively (determining the contributions of the corresponding particle–vacancy pair to the multiparticle excited state (8)).

The excited states of a multiparticle system with filled shells possessing spherical symmetry are characterized in the Russell–Saunders (LS) coupling approximation by the total angular momentum L and its projection M [41], therefore all single-particle particle–vacancy excitations have the same multipole in superposition (8).

To describe the optical properties of the given complexes, it is sufficient to consider only dipole transitions from the ground state $|\Phi_0\rangle$ to excited multiparticle states $|\Phi_k\rangle$ with $L = 1$, $M = 0$.

The amplitude coefficients $\mathbf{X}^{(k)}$ and $\mathbf{Y}^{(k)}$ in superposition (8) are determined by solving the RPAE matrix equation:

$$\mathbf{U}\mathbf{Z}^{(k)} = \hbar\Omega_k\mathbf{Z}^{(k)}, \tag{9}$$

where Ω_k are the eigenvalues of the matrix $\mathbf{U}$,

$$\mathbf{U} = \begin{pmatrix} \mathbf{A} & \mathbf{B} \\ -\mathbf{B}^* & -\mathbf{A}^* \end{pmatrix}, \ \mathbf{Z}^{(k)} = \begin{pmatrix} \mathbf{X}^{(k)} \\ \mathbf{Y}^{(k)} \end{pmatrix}. \tag{10}$$

The elements of Hermitian matrices $\mathbf{A}$, $\mathbf{B}$ are expressed in terms of single-particle energies E_i and Coulomb matrix elements of interparticle pair interaction, which are expressed as

$$\left\langle\alpha\beta\left|V\right|\gamma\eta\right\rangle = \delta_{\sigma_\alpha\sigma_\gamma}\delta_{\sigma_\beta\sigma_\eta}\int\varphi_\alpha^*(\mathbf{r})\varphi_\beta^*(\mathbf{r}')V(\mathbf{r},\mathbf{r}')\varphi_\gamma(\mathbf{r})\varphi_\eta(\mathbf{r}')d\mathbf{r}d\mathbf{r}', \tag{11}$$

with single-particle functions obtained by solving Eqs. (3), where the potential $V(\mathbf{r},\mathbf{r}')$ is determined from expansion (2).

Matrices $\mathbf{A}$ and $\mathbf{B}$ relate the single-particle excitations inside the electronic system [31, 37]:

$$\begin{gathered} A_{im,jn} = \delta_{ij}\delta_{mn}(E_n - E_i) + \left\langle in\left|U\right|mj\right\rangle, \\ B_{im,jn} = \left\langle ij\left|U\right|mn\right\rangle \end{gathered} \tag{12}$$

and include both direct (Hartree) and nonlocal exchange interactions, i.e.,

$$\left\langle\alpha\beta\left|U\right|\gamma\eta\right\rangle = 2\left\langle\alpha\beta\left|V\right|\gamma\eta\right\rangle + \left\langle\alpha\beta\left|V\right|\eta\gamma\right\rangle, \tag{13}$$

where the multiplier 2 before the direct component in this equality appears as a result of summation over spin variables.

The term containing the nonlocal exchange interaction in Eq. (13) was replaced by a matrix element in calculations of the excited states of the system in the random phase approximation with local exchange kernel (RPAX) [38],

$$\left\langle\alpha\beta\left|U\right|\gamma\eta\right\rangle = 2\left\langle\alpha\beta\left|V\right|\gamma\eta\right\rangle + \left\langle\alpha\beta\left|V_x\right|\gamma\eta\right\rangle, \tag{14}$$

where

$$V_x(\mathbf{r},\mathbf{r}') = \frac{\delta U_x\left[\rho(\mathbf{r})\right]}{\delta\rho(\mathbf{r})}\delta(\mathbf{r}-\mathbf{r}'), \tag{15}$$

(here the local exchange potential U_x is determined in accordance with expression (6)).

Positive eigenvalues Ω_k are the energies of transitions between the ground state $|\Phi_0\rangle$ and correlated excited states $|\Phi_k\rangle$. The energy spectra of excited states and the corresponding wave functions obtained by solving Eqs. (9), (10) allow to describe the processes associated with excitation of the system under various external influences. In particular, the response of the system to an external electromagnetic field is determined by the spectrum of dipole excitations.

The oscillator strengths f_k for dipole transitions between the ground and the kth excited state are equal to

$$f_k = 2m_e D_k^2 \Omega_k, \tag{16}$$

and satisfy the Thomas–Reich–Kuhn sum rule [37], i.e., $\sum_k f_k = N$.

Dipole matrix elements D_k (in the length form) are calculated by summing over all single-particle excitations [35, 36, 40]:

$$D_k = \sum_{im} \left(X_{im}^{(k)} d_{im} + Y_{im}^{(k)} d_{mi} \right), \tag{17}$$

where $d_{\alpha\beta} = \langle \alpha | z | \beta \rangle$ are the single-particle dipole amplitudes for the particle–vacancy pair.

The amplitude coefficients $\mathbf{X}^{(k)}$ and $\mathbf{Y}^{(k)}$ are normalized in accordance with the condition from [37], namely,

$$\sum_{im} \left(\left| X_{im}^{(k)} \right|^2 - \left| Y_{im}^{(k)} \right|^2 \right) = 1. \tag{18}$$

Results and discussion

Free charge carriers in semiconductor nanoparticles form electron shells regardless of the doping mechanism [42, 43]. On the other hand, it was established in [19], analyzing the distribution of electron densities of the ground states in cadmium selenide and cadmium sulfide nanocrystals (CdSe and CdS), that the type of doping determines the shell structure and its filling order, and, therefore, the density distribution of free charge carriers in the crystal bulk.

Coulomb repulsion between free electrons under surface doping shifts them towards the outer boundary of the system, and the characteristics of the electronic configuration induced by the surface doping mechanism ensure that only the angular degrees of freedom are excited during the formation of a collective dipole mode due to interaction with an external electromagnetic field. The motion of electrons in the radial direction is not included, since there is no effective restoring force acting on delocalized electrons from the positively charged core [26].

On the contrary, bulk-doped semiconductor nanocrystals are characterized by a more uniform distribution of electron density throughout the bulk, and the oscillation of free charges is translational in nature, similar to the situation in metal nanoparticles.

Surface doping

The step potential model [44, 45], replacing the potentials of individual atoms with an effective potential where delocalized conduction electrons move [46–48], implies that the electrons are strongly confined in their motion within the bulk of the nanoparticle under surface-type doping.

An example of surface-type doping is the method for photodoping nanocrystals used in [21, 22].

In this case, the external potential can be represented as a spherical potential well with impermeable walls [19, 22, 26]:

$$U_{ext}(r) = \begin{cases} -\dfrac{Ne^2}{\varepsilon_2 R}, & 0 < r < R, \\ -\dfrac{Ne^2}{\varepsilon_2 R} + U_0, & r > R, \end{cases} \tag{19}$$

where U_0 is some phenomenological parameter with the same order of magnitude as the electron work function of the semiconductor bulk material.

Calculations of the ground state of systems with closed electron shells with a different number of electrons N indicate that the distribution of electron density in surface-doped nanocrystals is considerably non-uniform, shifted towards the surface (see Fig. 1), which is qualitatively consistent with the predictions made in [19] based on the results of calculations performed in accordance with the density functional theory. This is due both to interelectronic Coulomb repulsion and to the peculiarities of the electronic structure of the system.

In the ground state, initial filling of electron shells with maximum orbital moments occurs, producing the following structure:

$$1s^2 2p^6 3d^{10} \ldots n_{\max} l_{\max}^{2(2l_{\max}+1)},$$

that is, all single-particle wave functions (7) of closed shells at $N \lesssim 10^2$ correspond to radial quantum numbers $n_r = n - l = 1$, for which the radial parts of the wave functions $P_{nl}(r)$ have no roots.

This electronic structure corresponds to the 'magic' numbers N for systems with closed electronic shells:

$$N = 2\left(l_{\max} + 1\right)^2,$$

where $l_{\max}$ is the angular momentum of the highest occupied molecular orbital (HOMO).

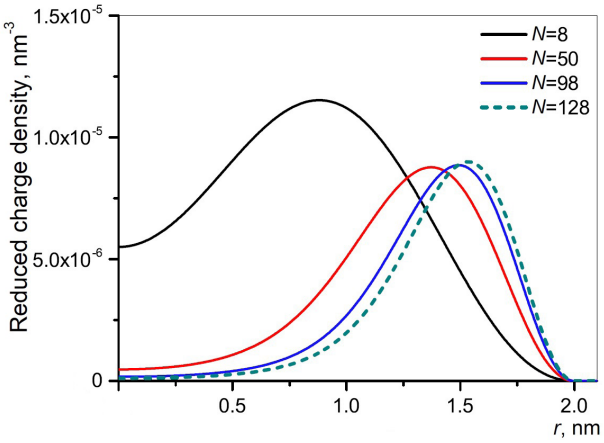

Fig. 1. Distributions of reduced electron charge density $\rho_e(r)/N$ in the bulk of surface-doped CdSe crystal for different numbers of electrons N

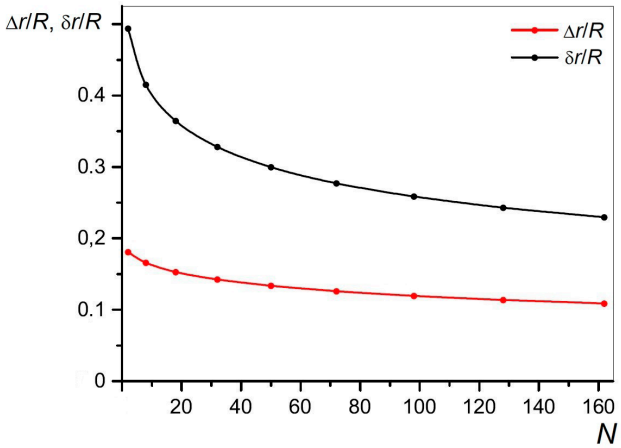

Fig. 2. Reduced displacement of the average radius of electronic system $\Delta r = \langle r \rangle / R$ and reduced effective width of electron layer $\delta r = \sqrt{\langle r^2 \rangle - \langle r \rangle^2}/R$ in the bulk of surface-doped CdSe crystal as functions of number of electrons

Fig. 2 shows the displacement ratio of the average electron radius to the nanocrystal radius $\Delta r = R - \langle r \rangle / R$ and the reduced effective width of electron density distribution $\delta r = \sqrt{\langle r^2 \rangle - \langle r \rangle^2}/R$. It can be seen that the dispersion of electron radius decreases with increasing number of electrons N, and the electronic system acquires a relatively narrow radial distribution, which determines its optical properties. At the same time, the distribution functions $\rho_e(r)$ calculated in the Hartree–Fock approximation (3) and using the local Dirac exchange potential (6) turned out to be almost identical for all selected values of N.

It was hypothesized in [19] that the dipole resonance observed in the photoabsorption spectrum of CdSe nanocrystals is transformed with an increase in the number of free charge carriers in the system from an excited state whose parameters are determined by size quantization into plasmon-type excitation, even with a relatively small crystal radius (R = 2 nm). Indeed, the harmonic plasmon resonance of rotational type also dominated in the spectra of dipole excitations of photodoped ZnO nanocrystals [21, 22] with a similar radial distribution of electron density. The collective nature of this resonance has been well described both within the quantum fluid oscillation model and within the quantum mechanical approach based on RPAE [26, 27].

However, the situation with cadmium selenide is radically different. As established in [27], a necessary condition for harmonic oscillations of electron density by the rotational plasmon type is that the size of the nanoparticle exceed the value of the effective Bohr radius a_0, which was satisfied for all nanoparticles considered in [21, 22]. On the other hand, this condition is not satisfied for CdSe nanocrystals, since R = 2 nm.

In view of this difference, we conducted an analysis of the optical properties of CdSe nanocrystals, which is presented below. The analysis provided conclusions about the nature of the dominant dipole resonance in CdSe photoabsorption spectra.

As established in the next section, the contribution to the collective excited state described by the wave function $|\Psi_k\rangle$ (see Eq. (8)) for nanoparticles with a uniform distribution of electron density, such as bulk-doped semiconductor nanocrystals, produces a sufficiently large number of particle–vacancy pairs, and the distribution of oscillator strengths in the optical spectrum is obtained as a result of numerical solutions of Eq. (10) taking into account the contribution of all single-particle excitations.

However, the situation is fundamentally different for surface-doped nanocrystals. Calculations indicate that a dominant expansion term appears in superposition (8) due to effective separation of the radial and angular motion of electrons, corresponding to the dipole transition between single-particle states on the lowest unoccupied (LUMO) and the highest occupied (HOMO) molecular orbitals with the excitation energy Δ:

$$\Delta = E_{\text{LUMO}} - E_{\text{HOMO}}.$$

In other words, only the states with the smallest radial quantum numbers n_r = 1 participate in the photoabsorption process, and only the transition between HOMO and LUMO electronic levels with the maximum angular moments $l_{\max}$ and $l_{\max}$ + 1, respectively, is effectively allowed for dipole excitations, while correlations between HOMO-LUMO single-particle excitation and other electron–hole pairs are negligible. This allows to describe the plasmon mode using the two-level model (proposed in [27]), where all single-particle transitions appear to be negligible, with the exception of the single HOMO-LUMO excitation.

In this case, the RPAE equation (10) is reduced to a system of two linear equations:

$$\begin{aligned} \left(\Delta + V_{TF} - \hbar\Omega\right) X + V_{TR} Y = 0, \\ \left(\Delta + V_{TR} + \hbar\Omega\right) Y + V_{TF} X = 0, \end{aligned} \tag{20}$$

where $V_{TF} = \langle in|v|mj\rangle$ is the forward-in-time matrix element between two single-particle particle–hole dipole excitations; $V_{TR} = \langle ij|v|mn\rangle$ is the backward-in-time matrix element between the ground state and the two-particle–two-hole excitation.

In the case of local exchange interaction (15), these matrix elements turn out to be equal to each other, $V_{TF} = V_{TR} = V$, and the RPAX 2×2 system of equations (20) has a simple analytical solution:

$$\hbar\Omega = \sqrt{\Delta^2 + 2\Delta V}, \tag{21}$$

$$X = \frac{\hbar\Omega + \Delta}{2\sqrt{\hbar\Omega\Delta}},\ Y = -\frac{\hbar\Omega - \Delta}{2\sqrt{\hbar\Omega\Delta}}. \quad (22)$$

As already mentioned, [19] discussed the transformation of dipole resonance in CdSe nanocrystals from size quantization to classical plasmon oscillations with increasing number of charge carriers in the system, even with its relatively small geometric dimensions ($R = 2$ nm). As demonstrated in [26, 27], the influence of Coulomb interaction determining the contribution of interparticle correlations to the collective excited state can be estimated by a dimensionless parameter written using the notations in Eq. (20) in the form:

$$\lambda = \Delta^2 / 2\Delta V = \Delta / 2V.$$

In the classical limit, with the system sizes significantly exceeding the Bohr radius, i.e., $R \gg a_0$, the Coulomb interaction dominates, and $\lambda \ll 1$. Conversely, in the size quantization mode, when $R \ll a_0$, the frequency Ω is mainly determined by the single-particle energy Δ ($\lambda \gg 1$). At the same time, analyzing Eq. (21), we can see that taking into account Coulomb correlations $2\Delta V$ causes the plasmon resonance to shift towards higher values compared with the energy of single-particle excitation Δ. Importantly, the shift of the excitation energy is not accompanied by any transformation of the wave function $|\Psi_\nu\rangle$, since it contains only electron–hole HOMO-LUMO pairs, which does not contradict the collective nature of this excited state. Indeed, superposition (8) contains a large number of terms, although the radial quantum numbers $n_r = 1$ and angular momenta $l_h = l_p - 1$ remain fixed, and summation is carried out over the angular momentum projections. Thus, the dipole excited state can be regarded as a collective mode if the number of free electrons in the filled HOMO shell participating in oscillatory motion is sufficiently large: $2(2l_{max} + 1) \gg 1$.

Another important parameter that allows to estimate the contribution of Coulomb correlations to excitation of the dipole mode is the ratio of the backward-in-time and forward-in-time amplitudes (Y and X, respectively):

$$\frac{Y}{X} = -\frac{\hbar\Omega - \Delta}{\hbar\Omega + \Delta} = -\frac{\sqrt{\Delta + 2V} - \sqrt{\Delta}}{\sqrt{\Delta + 2V} + \sqrt{\Delta}}. \quad (23)$$

In the case of small sizes of nanocrystals, when $R \ll a_0$ ($\lambda \gg 1$), the role of Coulomb correlations is negligible, $X \simeq 1$, $Y \ll 1$, because the energy of interelectronic interaction is small compared with the kinetic energy of electrons localized near an impenetrable potential barrier at the particle surface. The role of these correlations is especially important in the case of CdSe nanocrystals considered, when the effective mass of charge carriers is small compared with the free electron mass.

The approximation of independent single-particle electronic states describes both the ground state and the spectrum of dipole excitations sufficiently well in this size quantization mode. In another limiting case, at $R \gg a_0$ ($\lambda \ll 1$), the interelectronic interaction plays a significant role, which is confirmed by the relation $X \simeq -Y \simeq 1$. The increase in the back-in-time amplitude points to significant influence of Coulomb correlations in the ground state $|0\rangle$. The transformation of the uncorrelated ground state of the system formed from filled single-particle electronic states below the Fermi level into a correlated multiparticle ground state consists in simultaneous production of excited electron–hole pairs, corresponding in the case of a two-level model to transitions between single-particle HOMO and LUMO states. This transformation leads both to a noticeable shift in the excitation energy $\hbar\Omega$ and to a change in the dipole matrix element D that is the transition from the ground state to $|0\rangle$ the collective excited state $|1\rangle$. According to Eq. (21), Coulomb correlations lead to a significant increase in the transition energy $\hbar\Omega$ compared with its single-particle value Δ. Their ratio can be estimated as $\hbar\Omega/\Delta \simeq 2V/\Delta \simeq 1/\lambda$.

At the same time, as follows from Eq. (16), the dipole matrix element itself decreases. Since the ratio $X \simeq -Y$ holds true in the presence of correlations, the two terms on the right-hand side of this equation compensate for each other, which leads to a decrease in the multiparticle matrix element D compared with its single-particle value d. According to Eq. (21), the sum of the amplitudes X and Y is equal to

$$X + Y = \sqrt{\frac{\Delta}{\hbar\Omega}}. \tag{24}$$

Thus, a simultaneous decrease in the dipole matrix element and an increase in the transition energy $|0\rangle \rightarrow |1\rangle$ preserve the value of the oscillator strength, i.e.,

$$f = \frac{2m_e\Omega}{\hbar}|D|^2 = \frac{2m_e\Delta}{\hbar^2}|d|^2 = \frac{2}{3}N. \tag{25}$$

The strength of the transition oscillator $|0\rangle \rightarrow |1\rangle$ is 2/3 of the sum rule, which is a characteristic sign that this transition describes the contribution of the rotational dipole plasmon to the optical spectrum of the system. This conclusion is based on the property of the rotational mode: it includes only the angular motion of electrons; the radial degrees of freedom remain unexcited.

For the same reason, the square frequency of rotational plasmon is 2/3 of the square frequency of translational plasma oscillations observed in the case of bulk-type doping.

As an example, Fig. 3 shows the distribution of oscillator strengths in the vicinity of the dipole resonance for CdSe nanocrystal containing 98 delocalized electrons ($N = 98$) with a closed shell configuration

$$1s^2 2p^6 3d^{10} 4f^{14} 5g^{18} 6h^{22} 7i^{26}$$

and the maximum orbital moment $l_{max} = 6$ for the HOMO orbital. The figure illustrates the computational results obtained within the RPAE approximation by solving Eq. (10) with a complete set of particle–vacancy pairs. For comparison, the dashed line in the same figure shows the spectral position of the oscillator strength corresponding to the two-level model (20) for the HOMO → LUMO $7i \rightarrow 8j$ transition. The thin red line roughly corresponds to the profile of the photoabsorption cross section, generated by artificially broadening the spectral lines with Lorentzian profiles at a width of 0.2Ω. The energy position of the dominant resonance line on the spectrum (numbered 1) coincides with the analytical solution (21) with high accuracy, confirming the hypothesis that the resonance mode can be described as a correlated excited state including only transitions between HOMO and LUMO orbitals taking into account summation over all possible angular momentum projections.

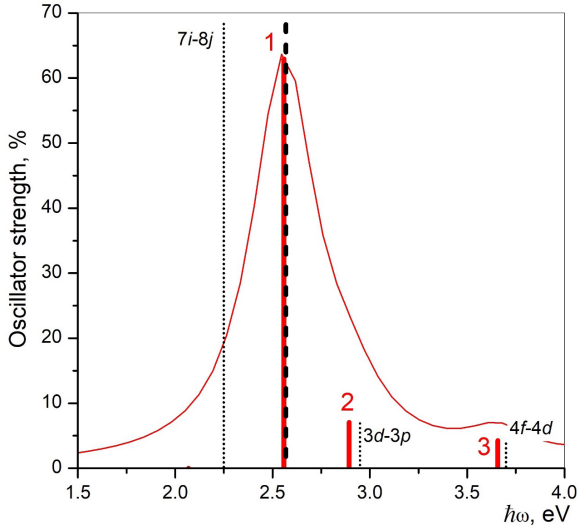

Fig. 3. Energy distribution of oscillator strengths in the vicinity of dipole resonance in CdSe nanocrystal ($N = 98$) according to different models: RPAE and single-particle Hartree–Fock approximations (bold solid red and dotted black lines, respectively), the two-level model (bold dashed black line). The spectral lines are numbered: $k = 1, 2, 3$

Notably, the oscillator strength includes 2/3 of the sum rule with a sufficiently high accuracy in both cases, allowing to classify the resonance mode as purely rotational oscillations. The graph in Fig. 3 also shows the oscillator strength, calculated in the single-particle approximation. According to Eq. (21), the shift of the resonance line 1 towards higher energies compared with the initial position of the energy $\Delta_{7i\to 8j}$, indicates the contribution of interparticle correlations to the formation of the resonance mode and confirms its collective nature. Dipole transitions whose lines are numbered 2 and 3 (containing 6 and 5% of the sum rule, respectively) correspond to transitions with excitation of radial degrees of freedom and bear a single-particle nature, judging by the small difference in their energies from the values in the Hartree–Fock approximation.

As an addition to analysis of the dipole spectrum in Fig. 3, Fig. 4 shows for comparison the radial distribution of electron density for the ground state of the system $\rho_e(r)$ and the radial distributions of transition density for spectral lines 1, 2 and 3, illustrating the fundamental difference between the two types of excited states. The given radial distributions for lines 1, 2 and 3 are defined as

$$\rho_{tr}^{(k)}(r) = \sum_{im}\left(X_{im}^{(k)}\phi_i(r)\phi_m^*(r) + Y_{im}^{(k)}\phi_i^*(r)\phi_m(r)\right). \tag{26}$$

The same graph (see Fig. 4) shows the density of the dipole transition for the two-level model, which in this case is defined as

$$\langle HOMO \,|\, LUMO\rangle = P_{7i}(r)P_{8j}(r).$$

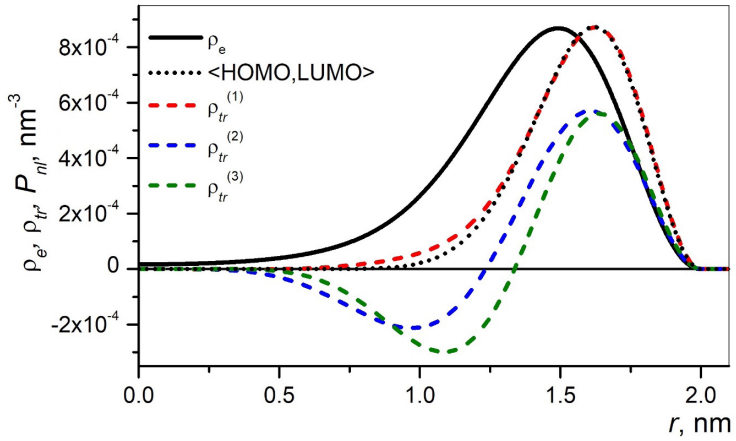

Fig. 4. Radial distributions of electron density $\rho_e(r)$ and transition density $\rho^{(k)}{}_{tr}(r)$ for spectral lines with k = 1, 2, 3 (see Fig. 3), as well as the overlap of wave functions $P_{nl}(r)$ for molecular orbitals $1i_{(HOMO)}$ and $1j_{(LUMO)}$

As seen from the presented dependences, the transition density of resonance line 1 almost completely coincides with the data of the two-level model and is concentrated on the outer boundary of the electron density distribution, while the densities of single-particle transitions 2 and 3 are more evenly distributed throughout the entire bulk of the system, since they correspond to excitation of radial degrees of freedom.

On the other hand, in our opinion, the transformation of resonant dipole mode in CdSe nanocrystals as the number of electrons increases with relatively small geometric dimensions of the system cannot be characterized as a transition from the quantum to the classical mode, as suggested in [19]. Despite the increase in the shift of the position of the resonance line relative to the energy of the single-particle transition Δ observed in Fig. 5,*a*, the values of the parameter λ and the amplitude ratio $-Y/X$ (see Fig. 5, *b*, *c*) obtained for all $N \lesssim 10^2$ still do not satisfy the

conditions $\lambda \ll 1$ and $X \simeq -Y \simeq 1$, characteristic of classical plasmon oscillation, when the energy of the Coulomb interelectronic interaction prevails in the correlated multiparticle excitation over the single-particle energy of size quantization Δ. This is a consequence of the relatively small effective electron mass in the CdSe and, accordingly, the large effective Bohr radius. While the relative increase in the back-in-time amplitude observed in Fig. 5,*c* indicates a corresponding increase in the contribution of Coulomb correlations to the ground state $|\Phi_0\rangle$ as the number of particles N increases, it turns out to be insufficient for transition to the classical oscillations of the electronic system.

In this case, the transition of resonant excitations from the quantum to the classical mode is achieved by increasing the geometric dimensions of the nanocrystal so that at least the condition $R > a_0$ is satisfied. Fig. 6 shows the dependences for the main parameters of the resonant excited state on the radius R in a nanocrystal containing 98 electrons ($N = 98$) for the resonance mode corresponding to spectral line 1 in Fig. 3. Evidently, the transition of the rotational plasmon mode to the classical regime in the case of CdSe is achieved at values of R above 6 nm, i.e., at least for $R \gtrsim a_0$.

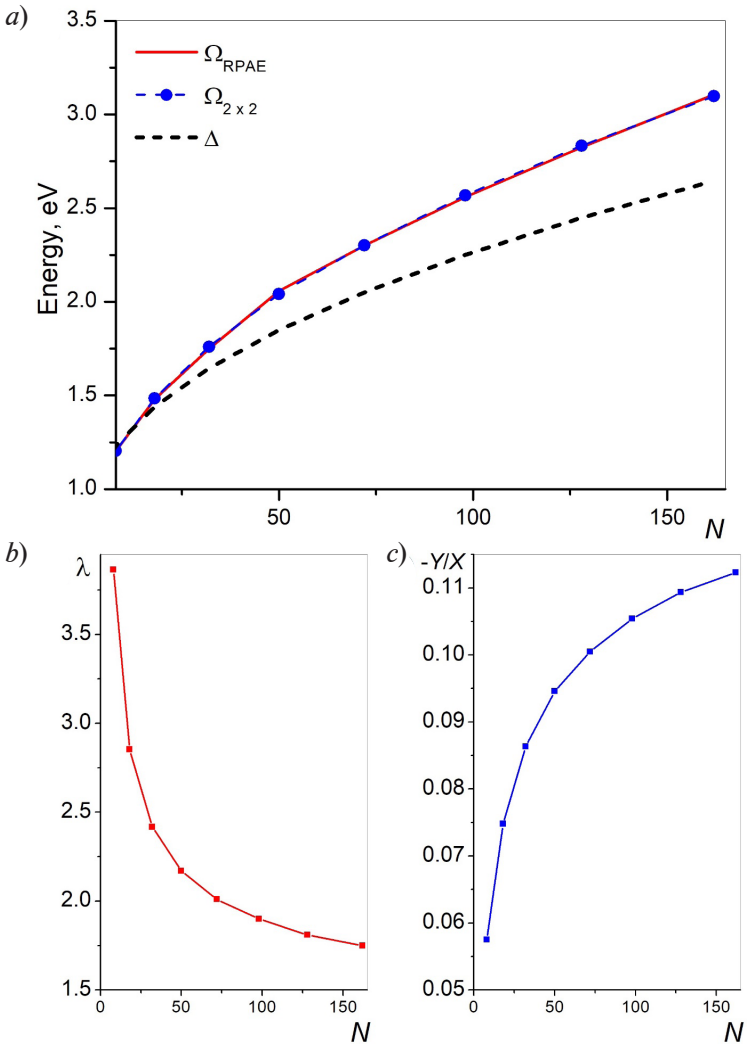

Fig. 5. Main parameters of resonant excited state in a nanocrystal as functions of the number of electrons N: plasmon energies $\hbar\Omega$ obtained in different approximations (*a*); parameter λ (*b*) and amplitude ratios $-Y/X$ (*c*).
RPAE approximations, two-level model (2×2) and one-particle approximation (Δ) (Fig. 5,*a*) are used

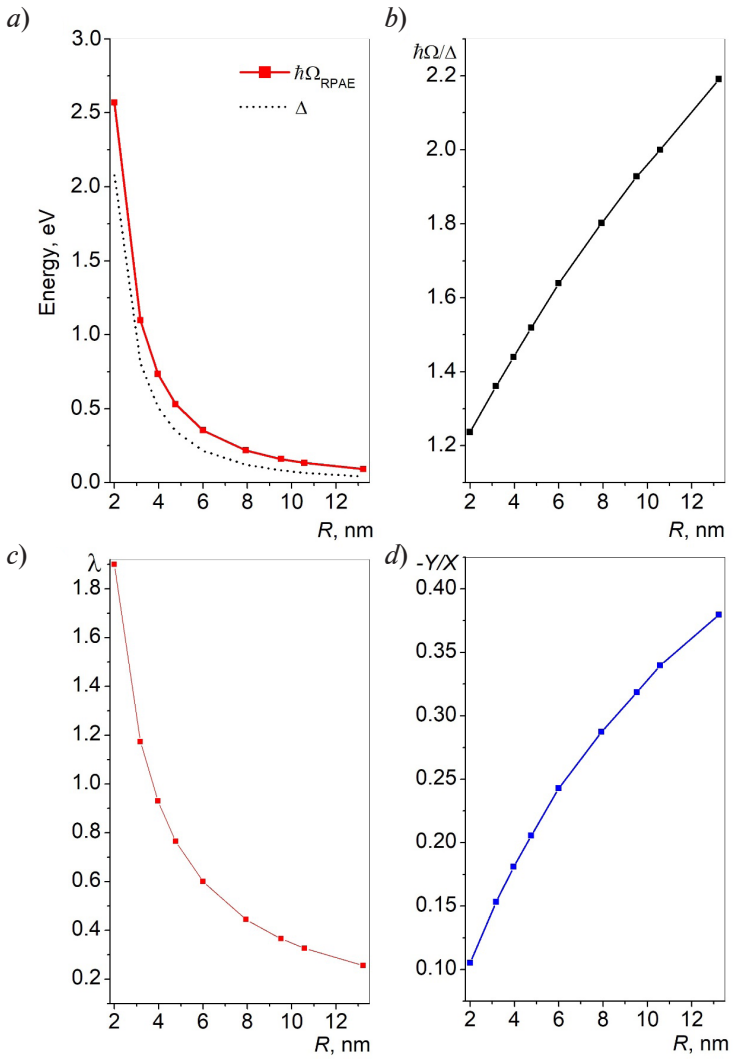

Fig. 6. Main parameters of resonant excited state in CdSe nanocrystal ($N = 98$) as function of potential well radius R: dipole resonance energy $\hbar\Omega$ and energy difference of single-particle levels Δ (*a*), ratio $\hbar\Omega/\Delta$ (*b*), parameter λ (*c*) and ratio $-Y/X$ for resonant line 1 (see Fig. 3) (*d*)

Bulk doping

In the case of bulk doping of semiconductor nanocrystals, the positive charge is assumed to be uniformly distributed throughout the entire bulk of the system [19] and the external potential it generates within the model used should take the form of the potential of a uniformly charged sphere with the charge $Z = Ne$ in a dielectric environment:

$$U_{ext}(r) = \begin{cases} \dfrac{Ne^2}{2\varepsilon_1 R^3}\left(r^2 - \left(1 + \dfrac{2\varepsilon_1}{\varepsilon_2}\right)R^2\right), & 0 < r < R, \\ -\dfrac{Ne^2}{\varepsilon_2 r} + U_0, & r > R. \end{cases} \tag{27}$$

Transformation of the external potential in the case of bulk-type doping compared with the surface-type leads to a significant change in the structure of the electronic shells of the system, their filling order and, consequently, the distribution of electron density in the bulk of the

nanocrystal. The calculations show that the order of shell filling in bulk-doped systems both in the Hartree–Fock approximation and using the local exchange potential (6) should be similar to this order for delocalized electrons in clusters of alkali metal atoms within the jellium model [6, 9, 46, 49, 50], when delocalized conduction electrons move in the field of the effective potential of a uniformly charged ion core. Thus, the electronic structure of the ground state of a bulk-doped nanocrystal containing 124 electrons is written as follows:

$$1s^2 2p^6 3d^{10} 2s^2 4f^{14} 3p^6 5g^{18} 4d^{10} 6h^{22} 3s^2 7i^{26} 4p^6.$$

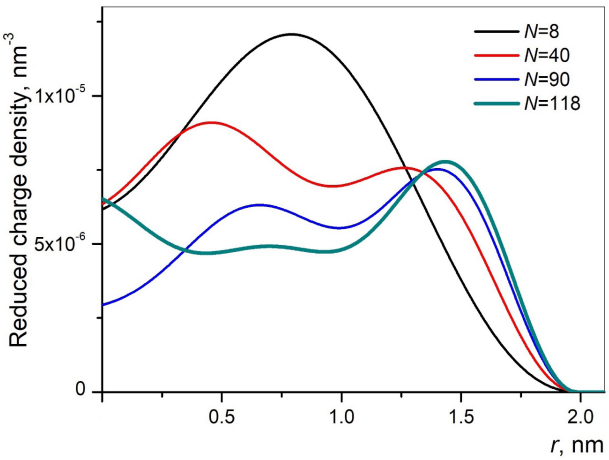

Fig. 7. Reduced radial distributions of electron density $\rho_e(r)/N$ in bulk-doped CdSe nanocrystals with a different number of electrons N

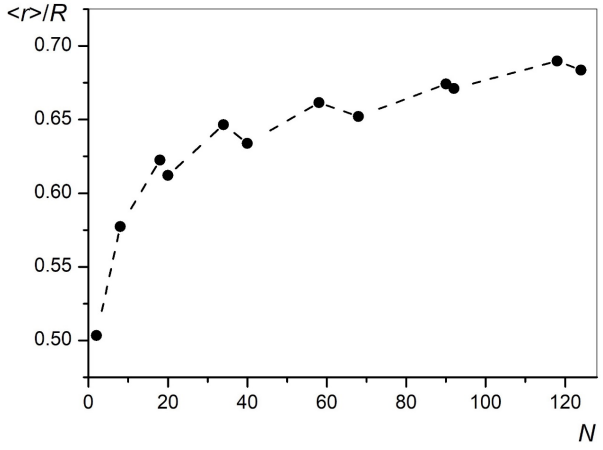

Fig. 8. Ratio of average radius of electronic system to radius of nanocrystal $\langle r \rangle / R$ as function of system particle number

In other words, unlike the situation with surface-type doping discussed in the previous section, as shells are filled, orbitals whose radial wave functions $P_{nl}(r)$ have no roots alternate with orbitals whose wave functions have roots, which, in turn, leads to a more uniform distribution of electron density $\rho_e(r)$ over the bulk of the system (Fig. 7). Fig. 8 shows a noteworthy non-monotonic dependence of the average radius of the electronic system on the number of particles. The reason why steps appear, accompanied by a slow increase in $\langle r \rangle$, is that the filled shells alternately have radial wave functions $P_{nl}(r)$ with no roots, characterized by greater average radii, and wave functions with roots (this was not observed in the case of surface-doped systems).

As in the case of surface doping, the resonance mode dominates in the spectrum of dipole excitations of bulk-doped nanocrystals; its frequency significantly shifted relative to the positions of the frequencies of single-particle transitions.

Fig. 9 shows the distributions of oscillator strengths in the CdSe crystal with 90 electrons ($N = 90$) and the ground state configuration

$$1s^2 2p^6 3d^{10} 2s^2 4f^{14} 3p^6 5g^{18} 4d^{10} 6h^{22}$$

in the vicinity of dipole resonance, calculated in the random phase approximation both taking into account the nonlocal exchange interaction (RPAE) and the local exchange potential (15) (RPAX). It should be noted that unlike surface doping, in the case of bulk doping, electrons under dipole resonance move in the direction normal to the system surface with minor deviations in the distribution of electron density relative to its ground state. On the other hand, oscillations of the electronic system under surface-type doping have a compressive nature, with significant variation in the charge density occurring during motion [27]. As established above, the reason for this is that only angular (rotational) degrees of freedom participate in excitation of the collective mode under surface-type doping.

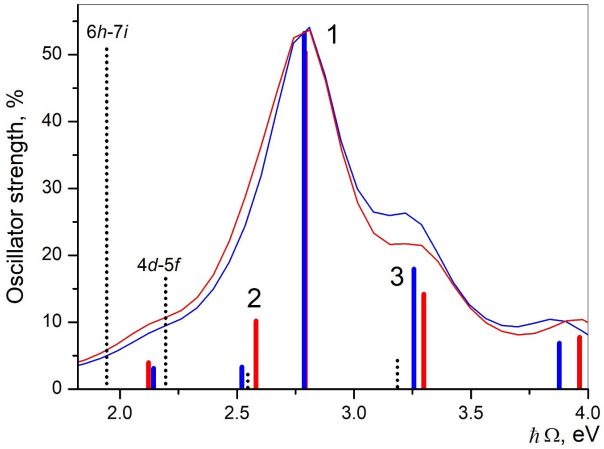

Fig. 9. Energy distributions of oscillator strengths in the vicinity of dipole resonance in the spectrum of bulk-doped CdSe nanocrystal ($N = 90$) obtained in different approximations: RPAE and RPAX (vertical red and blue segments, respectively), single-particle Hartree–Fock approximation (vertical black dotted lines).
The spectral lines are numbered: $k = 1, 2, 3$

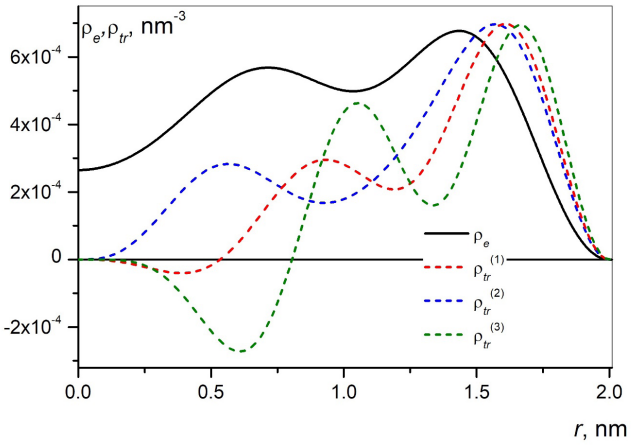

Fig. 10. Radial distributions of electron density $\rho_e(r)$ and transition density $\rho_{tr}^{(k)}(r)$ for spectral lines with $k = 1, 2, 3$ (see Fig. 9)

The motion of electrons in the direction normal to the system surface in the case of bulk doping is due to the fact that an effective restoring force acting on delocalized electrons arises in the parabolic potential generated by the bulk distribution of the positive charge in the nanocrystal.

Within the adiabatic approximation [24, 25], such collective excitation is identical in nature to the surface plasmon in the spectra of metal clusters [6, 9, 46] and can be described as harmonic oscillations in the center of mass of an electron cloud in the parabolic potential of a positively charged core. At the same time (see Fig. 9), pronounced fragmentation is observed in the resonance line due to the interaction of the harmonic mode with single-particle excitations. In contrast with the situation discussed in the previous section, a difference appeared in the position of the lateral maxima, associated with different exchange potentials, preserving an almost unchanged position of the central peak and its oscillator strength. This result confirms the link between the fragmentation of the resonance line and the interparticle interaction involving the exchange component.

Fig. 10 shows the radial distributions of electron density of the ground state $\rho_e(r)$ and the density of dipole transitions for the spectral lines numbered in Fig. 9. Importantly, the transition density dramatically differs from zero over the entire bulk of the system for all three spectral lines, including the main one numbered 1. This means that at least several particle–vacancy pairs participate in the formation of collective modes (8) and the two-level model (20) is no longer applicable.

The table gives the values of the forward-in-time and backward-in-time amplitudes for the main single-particle transitions that contribute to the corresponding lines in the spectrum of excited states in a cadmium selenide nanocrystal with the number of electrons $N = 90$, shown in Fig. 9. As can be seen from the data in the table, all three dipole perturbations (including the main resonance line 1 with an energy of $\hbar\Omega = 2.8$ eV and an oscillator strength of approximately 52% of the sum rule) are linear combinations (8), where the main contribution is made by two single-particle transitions: $6h \to 7i$ and $4d \to 5f$. The influence of other particle–vacancy pairs turned out to be insignificant. Judging by the amplitude ratios $-Y/X \sim 1$, correlations in the ground states play a significant role in all cases, so we can conclude that all three lines can be regarded as the result of fragmentation of one harmonic mode.

Table

Calculated amplitudes of the main single-particle transitions contributing to spectrum of excited states in CdSe nanocrystal (see Fig. 9)

Spectral line	Amplitudes, arb. units, or their ratios for transition					
	$6h \to 7i$			$4d \to 5f$		
	X	$-Y$	$-Y/X$	X	$-Y$	$-Y/X$
1	0.60	0.12	0.20	0.54	0.07	0.13
2	0.36	0.05	0.14	0.44	0.04	0.09
3	0.22	0.05	0.23	0.15	0.03	0.20

Notations: X, Y are the forward-in-time and backward-in-time amplitudes, respectively. Note. The number of electrons in the electron shell was assumed to be $N = 90$.

Fig. 11,*a* shows the $\hbar\Omega_{\text{RPAE}}$ dependences for the energy of the resonance mode on the number of delocalized electrons, calculated in the random phase approximation with a full basis of single-particle excitations, as well as the computational results obtained within the two-level model for transitions with the maximum oscillator strength $\Omega_{2\times2}$ and the energy of the corresponding single-particle transitions Δ depending on the number of electrons in bulk-doped CdSe nanocrystals. In contrast to the situation with surface-type doping, where, according to the data presented in Fig. 5, the results obtained by the two-level model and the calculations taking into account the full basis virtually coincided, there is a significant discrepancy between these approaches for any number of electrons in the system. This confirms the significant influence

of correlations between single-particle channels on the formation of a collective excited state (8). This influence is also confirmed by the observation that the frequency Ω_{RPAE} is increased by almost two times compared with the frequency of the single-particle transition Δ, while the amplitude ratio $-Y/X$ for the main dipole transitions is higher by more than two times (compared with the results in Fig. 5,*a*). Recall that this ratio serves as an indicator of correlations in the ground state.

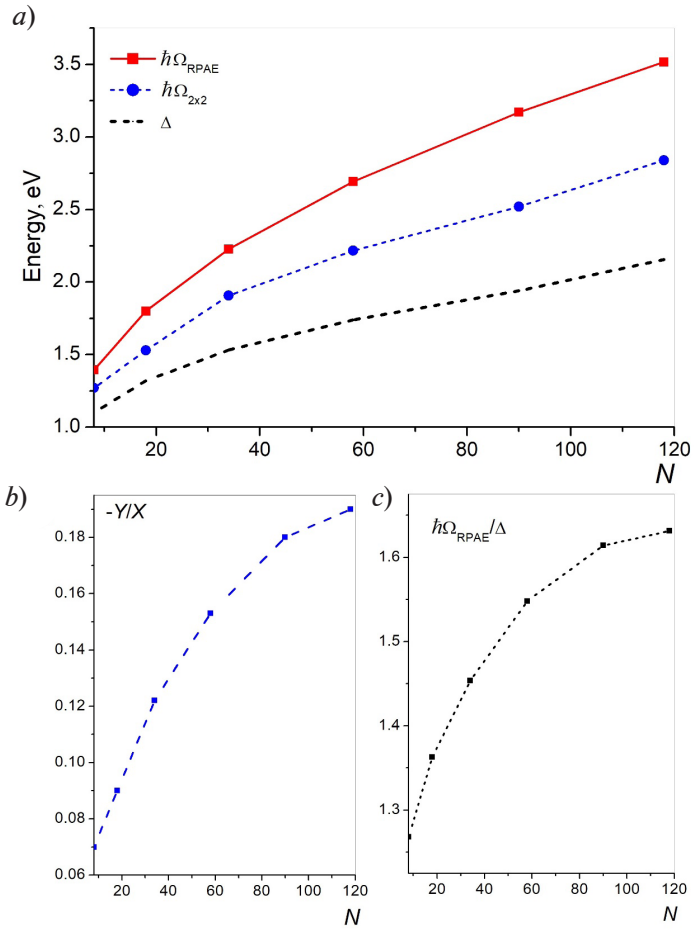

Fig. 11. Main parameters of resonant excited state in bulk-doped CdSe nanocrystal as function of number of electrons N: dipole resonance frequencies Ω obtained in different approximations (*a*); amplitude ratios $-Y/X$ (*b*) and ratios $\hbar\Omega_{RPAE}/\Delta$ (*c*). RPAE approximations, two-level model (2 × 2) and one-particle approximation (Δ) were used (Fig. 11,*a*)

Thus, the collective dipole mode in CdSe nanocrystals with bulk-type doping exhibits all the properties of a correlated multiparticle excited state. Therefore, it can be described as a surface plasmon resonance, even though the condition $X \simeq -Y \simeq 1$ is not satisfied for the considered case when $R = 2$ nm at $N \lesssim 10^2$.

As in the case of surface doping, the collective resonance mode increasingly approaches the classical plasmon in its properties with an increase in the geometric dimensions of the bulk-doped nanocrystal. Fig. 12,*a* shows the dependences for the energy of the resonant excited state $\hbar\Omega_{RPAE}$ and the differences of single-particle energy levels Δ for the single-particle transition $6h \rightarrow 7i$ (HOMO → LUMO) on the radius R in a nanocrystal containing $N = 90$ electrons for the resonance mode corresponding to line 1 in Fig. 9,*a*. Fig. 12,*a* also shows the analytical radial dependence of the classical frequency of plasma oscillations Ω_{cl} for a conducting sphere in a dielectric environment; the graph is plotted by the formula [12]:

$$\Omega_{cl} = \sqrt{\frac{3e^2 N}{m\left(\varepsilon_1 + 2\varepsilon_2\right) R^3}}. \tag{28}$$

As seen from this graph, there is still a noticeable discrepancy between the frequency of the dipole resonance obtained by quantum mechanical calculations and by the classical estimate at $R = 2$ nm. However, its magnitude decreases rapidly, a transition from the quantum regime of plasma oscillations to the classical one can be assumed to be already made at $R \gtrsim 4$ nm, when the influence of interparticle interaction in the electronic system prevails over the effects of size quantization, and the ground state in this case is a highly correlated system. This is also evidenced by the dependences presented in Fig. 12,*b* and *c* for the ratios of energies and amplitudes for the electronic transition making the main contribution to the sum (8).

Thus, we can conclude that the conditions for the transition of collective dipole excitation from the quantum regime to the classical one largely depend not only on the geometric dimensions of the nanocrystal and the number of free charge carriers, but also on the doping type; in the case of bulk doping, the transition is observed at relatively smaller values of the system radius.

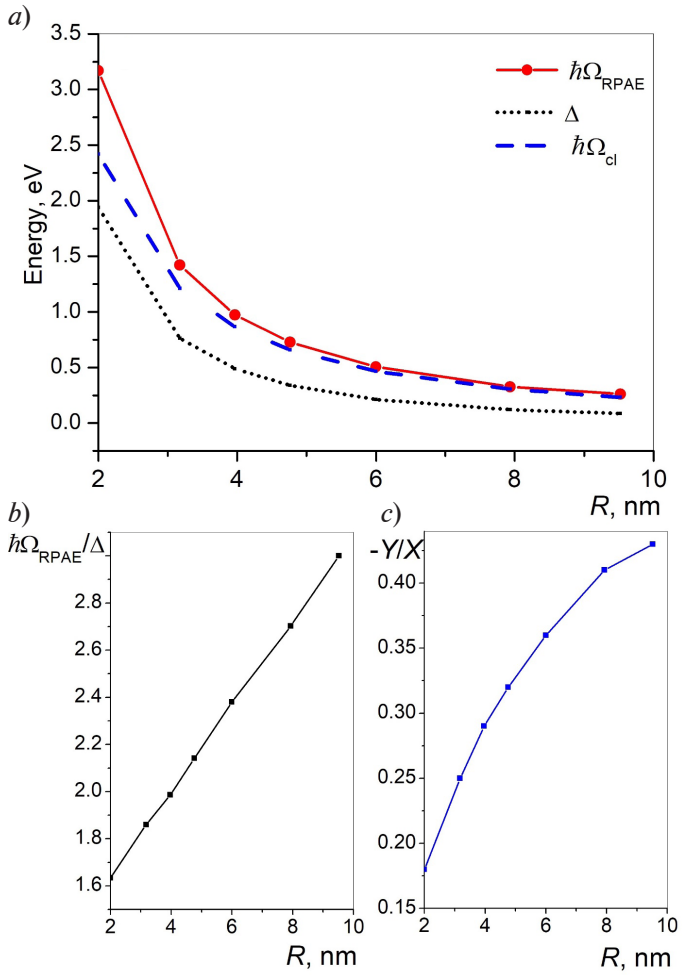

Fig. 12. Radial dependences for main parameters of the resonant excited state in bulk-doped CdSe nanocrystal ($N = 90$): dipole resonance energies $\hbar\Omega$ according to different models (*a*), as well as $\hbar\Omega_{\mathrm{RPAE}}/\Delta$ (*b*) and amplitude $-Y/X$ (*c*) ratios. RPAE and single-particle (Δ) approximations are used; the figure also shows the corresponding values of the classical plasmon resonance frequency Ω_{cl} (see Fig. 12,*a*)

Conclusion

The paper theoretically investigated the optical properties of semiconductor nanocrystals with different types of doping. We considered cadmium selenide (CdSe) nanocrystals containing different numbers of delocalized charge carriers. The interaction processes of electrons with each other and with an external electromagnetic field were described using a theoretical approach based on the Hartree–Fock approximation and the random phase approximation taking into account exchange interactions (RPAX). For comparison, the results are also presented for calculations in the local density approximation with the Dirac–Slater potential.

It was found that a dominant resonance line is observed in the optical spectra of nanocrystals obtained using both approaches; its position practically does not depend on the method chosen for describing the exchange interaction between electrons for all the given particle numbers in the system. The excited state corresponding to the resonant dipole transition has a collective nature in both surface and bulk doping mechanisms, as evidenced by the significant contribution of multiparticle correlations to the generation of the wave function.

In the case of surface doping, the electronic structure of the ground state has a largely non-uniform distribution of charge density, when the maximum of the distribution function is shifted to the surface of the nanocrystal, which, in turn, determines the nature of the oscillations of the dipole resonance mode.

Analyzing the distribution of oscillator strengths in the vicinity of the resonance line, as well as the corresponding dipole amplitudes and the density distribution of dipole transitions, we found that the oscillations of electron density in the collective mode are rotational in nature, with only angular degrees of freedom excited, while the motion in the radial direction is practically frozen, since there is no restoring force (directed along the normal to the surface) acting on charge carriers in the external potential.

This conclusion is further corroborated by the results obtained within the two-level model that describes the dipole resonance under surface doping as a correlated excited state composed of particle–vacancy pairs including only transitions between HOMO and LUMO orbitals for all possible angular momentum projections. Calculations indicate that the resonance frequency values obtained taking into account all possible single-particle transitions and within the two-level model turn out to be nearly identical for all CdSe nanocrystals considered containing from 8 to 162 delocalized electrons. Since the relationship between the rotational mode and single-particle excitations involving radial degrees of freedom is weak, the resonance line is virtually not fragmented. It was also found for relatively small system sizes, when the radius of the nanocrystal turns out to be less than the effective Bohr radius, that the resonance mode still does not make a transition from size quantization mode to classical plasmon oscillations with an increase in the number of electrons, even despite the increasing contribution of interelectron Coulomb interaction. The tendency towards transition to classical mode is manifested only when the radius of the system is increased to the size of the effective Bohr radius, with the rotational character of oscillatory motion preserved.

As established by the calculations, the electronic structure of the ground state turns out to be significantly different for bulk doping compared with surface-doped systems. In this case, the radial distribution of electron density over the bulk of the nanocrystal becomes more uniform, and the parabolic nature of the positively charged core induces a radially directed restoring force acting on the electrons. Therefore, the collective excited state can be described as harmonic oscillations of the electron cloud as a whole in the direction normal to the surface of the system with minor deviations in the density distribution compared with the ground state.

Thus, in the case of bulk doping, the dipole resonance can be described as a collective translational mode where, in contrast with surface doping, several single-particle dipole transitions are correlated simultaneously. This is confirmed by the fact that the results obtained by the two-level model differ significantly from those taking into account the full single-particle basis, and the difference increases as the number of particles in the system increases. In addition, the interaction of the harmonic mode with single-particle excited states leads to fragmentation of the resonance line, since the degrees of freedom of the oscillatory electronic system are not separated in this situation. Quantum effects also make the largest contributions to forming the collective mode at relatively small sizes of nanocrystals, however, the transition to the classical plasmon oscillation mode occurs at smaller radii of the system than with the surface type of doping. As a result, the

dipole oscillations of the electron cloud can be described as a plasmon mode even at sizes comparable to the effective Bohr radius. The frequency of this mode tends to the classical frequency of plasma oscillations in a spherical conductor.

Thus, it can be concluded that the optical spectrum of semiconductor nanocrystals is dominated by a resonant dipole mode regardless of the method used for doping. The nature of the mode in question is determined by the size of the system itself, as well as the type and degree of doping, i.e., the number of delocalized charge carriers. As the geometric dimensions of the electronic system (primarily) and the number of its electrons increase, a power-law transition of the collective excited state occurs from the size quantization mode to classical plasmon oscillatory motion of this system. In this case, the nature of motion depending on the number of excited degrees of freedom is determined by the electronic structure of the ground state. In turn, the electronic structure of this state is formed in accordance with the distribution of the positive charge potential, i.e., with the doping type.

REFERENCES

1. **Klimov V. V.,** Nanoplasmonics, Jenny Stanford Publishing, New York, 2014.

2. **Bozhevolniy S. I.**, **Martin-Moreno L., Garcia-Vidal F.** (Eds.), Quantum plasmonics (Springer Series in Solid-State Sciences. Vol. 185), Springer International Publishing, Cham, Switzerland, 2017.

3. **Enoch S., Bonod N.,** Plasmonics: From basics to advanced topics. (Springer Series in Optical Sciences. Vol. 167), Springer-Verlag, Heidelberg, Berlin, 2012.

4. **Tame M. S., McEnery K. R., Özdemir Ş. K., et al.,** Quantum plasmonics, Nat. Phys. 9 (June) (2013) 329–340.

5. **Scholl J. A., Koh A. L., Dionne J. A.,** Quantum plasmon resonances of individual metallic nanoparticles, Nature. 483 (22 March) (2012) 421–427.

6. **Brack M.,** The physics of simple metal clusters: Self-consistent jellium model and semiclassical approaches, Rev. Mod. Phys. 65 (3) (1993) 677–732.

7. **Harb M., Rabilloud F., Simon D., et al.,** Optical absorption of small silver clusters: Ag_n ($n = 4–22$), J. Chem. Phys. 129 (19) (2008) 194108.

8. **Xuan F., Guet C.,** Core-polarization-corrected random-phase approximation with exchange for dipole surface plasmons in silver clusters, Phys. Rev. A. 94 (4) (2016) 043415.

9. **Kreibig U., Vollmer M.,** Optical properties of metallic clusters (Springer Series in Materials Science. Vol. 65), Springer-Verlag, Heidelberg, Berlin, 1995.

10. **Kreibig U., Zacharias P.,** Surface plasma resonances in small silver and gold particles, Z. Physik. 231 (2) (1970) 128–143.

11. **Kriegel I., Scotognella F., Manna L.,** Plasmonic doped semiconductor nanocrystals: Properties, fabrication, applications and perspectives, Phys. Rep. 674 (28 February) (2017) 1–52.

12. **Klimov V. I.,** Nanocrystal quantum dots, Second edition, CRC Press, Boca Raton, Florida, USA, 2010.

13. **Monreal R. C., Antosiewicz T. J., Appel S. P.,** Competition between surface screening and size quantization for surface plasmons in nanoparticles, New J. Phys. 15 (8) (2013) 083044.

14. **Scotognella F., Della Valle G., Kandada A. R. S., et al.,** Plasmonics in heavily-doped semiconductor nanocrystals, Eur. Phys. J. B. 86 (4) (2013) 154.

15. **Xie Y., Carbone L., Nobile C., et al.** Metallic-like stoichiometric copper sulfide nanocrystals: Phase- and shape-selective synthesis, near-infrared surface plasmon resonance properties, and their modeling, ACS Nano. 7 (8) (2013) 7352–7369.

15. **Xie Y., Carbone L., Nobile C., et al.** Metallic-like stoichiometric copper sulfide nanocrystals: Phase- and shape-selective synthesis, near-infrared surface plasmon resonance properties, and their modeling // ACS Nano (The American Chemical Society). 2013. Vol. 7. No. 8. Pp. 7352–7369.

16. **Routzahn A. L., White S. L., Fong L.-K., Jain P. K.,** Plasmonics with doped quantum dots, Isr. J. Chem. 52 (11–12) (2012) 983–991.

17. **Luther J. M., Jain P. K., Ewers T., Alivisators A. P.,** Localized surface plasmon resonances arising from free carriers in doped quantum dots, Nat. Mater. 10 (May) (2011) 361–366.

18. **Faucheaux J. A., Stanton A. L. D., Jain P. K.,** Plasmon resonances of semiconductor nanocrystals: Physical principles and new opportunities, J. Phys. Chem. Lett. 5 (6) (2014) 976–985.

19. **Zhang H., Kulkarni V., Prodan E., et al.,** Theory of quantum plasmon resonances in doped semiconductor nanocrystals, J. Phys. Chem. C. 118 (29) (2014) 16035–16042.

20. **Lounis S. D., Runnerstrom E. L., Bergerud A., et al.,** Influence of dopant distribution on the plasmonic properties of indium tin oxide nanocrystals, J. Am. Chem. Soc. 136 (19) (2014) 7110–7116.

21. **Schimpf A. M., Thakkar N., Gunthardt C. E., et al.,** Charge-tunable quantum plasmons in colloidal semiconductor nanocrystals, ACS Nano. 8 (1) (2014) 1065–1072.

22. **Schimpf A. M., Gunthardt C. E., Rinehart J. D., et al.,** Controlling carrier densities in photochemically reduced colloidal ZnO nanocrystals, J. Am. Chem. Soc. 135 (44) (2013) 16569–16577.

23. **Liu X., Swihart M. T.,** Heavily-doped colloidal semiconductor and metal oxide nanocrystals, an emerging new class of plasmonic nanomaterials, Chem. Soc. Rev. 43 (11) (2014) 3908–3920.

24. **Gerchikov L. G., Guet C., Ipatov A. N.,** Multiple plasmons and anharmonic effects in small metallic clusters, Phys. Rev. A. 66 (5) (2002) 053202.

25. **Ipatov A. N., Gerchikov L. G., Guet C.,** Resonant photoabsorption of metallic clusters in a strong laser field, Comput. Mater. Sci. 35 (3) (2006) 347–353.

26. **Ipatov A. N., Gerchikov L. G., Guet C.,** Plasmon resonance in photoabsorption of colloidal highly doped ZnO nanocrystals, Nanoscale Res. Lett. 13 (1) (2018) 297.

27. **Ipatov A. N., Gerchikov L. G.,** Rotational dipole plasmon mode in nanoscale semiconductor particles, J. Exp. Theor. Phys., 132 (6) (2021) 922–940.

28. **Yabana K., Bertsch G. F.,** Electronic structure of C_{60} in a spherical basis, Phys. Scr. 48 (5) (1993) 633–637.

29. **Ju N., Bulgac A., Keller J. W.,** Excitation of collective plasmon states in fullerenes, Phys. Rev. B. 48 (12) (1993) 9071–9079.

30. **Ostling P., Apell P., Rosén A.,** Theory for collective resonances of the C_{60} molecule, Europhys. Lett. 21 (5) (1993) 539–544.

31. **Madjet M., Guet G., Johnson W. R.,** Comparative study of exchange-correlation effects on electron and optical properties of alkali-metal clusters, Phys. Rev. A. 51 (2) (1995) 1327–1339.

32. **Mukherjee D.,** Applied many-body methods in spectroscopy and electronic structure, Springer, NY, 1992.

33. **Serra Ll., Garcias F., Navarro J., et al.,** Electronic surface excitations of cavities in metals, Phys. Rev. B. 46 (15) (1992) 9369–9379.

34. **Varshalovich D. A., Moskalev A. N., Khersonskii V. K.,** Quantum theory of angular momentum, World Scientific, Singapore, 1988.

35. **Ipatov A. N., Gerchikov L. G.** Many-particle correlations in microscopic electron-hole droplets, J. Phys. B. – At. Mol. Opt. 47 (18) (2014) 185101.

36. **Gerchikov L. G., Ipatov A. N.,** Collective excitations in the optical spectra of nanoscale exciton and electron-positron droplets, J. Exp. Theor. Phys. 119 (5) (2014) 891–901.

37. **Amusia M. Y., Chernysheva L.V.,** Computation of atomic processes. A handbook for the atom programs, CRC Press, Boca Raton, 1997.

38. **Dreizler R. M., Gross E. K. U.,** Density functional theory: An approach to the quantum many-body problem, Springer, Berlin, 1990.

39. **Landau L. D., Lifshitz E. M.,** Quantum mechanics. Non-relativistic theory. (Course of theoretical physics. Vol. 3), Pergamon Press, Oxford, London, New York, Paris, 1965.

40. **Ipatov A. N., Gerchikov L. G.,** Stability and properties of finite Fermi-systems with different masses, J. Exp. Theor. Phys. 118 (1) (2014) 93–103.

41. **Sobel'man I. I.**, Introduction to the theory of atomic spectra (International Series in Natural Philosophy, Vol. 40), Pergamon Press, Oxford, UK, 1972.

42. **Banin U., Cao Y., Katz D., Millo O.,** Identication of atomic-like electronic states in indium arsenide nanocrystal quantum dots, Nature. 400 (5 August) (1999) 542–544.

43. **Kouwenhoven L. P., Austing D. G., Tarucha S.,** Few electron quantum dots, Rep. Progr. Phys. 64 (6) (2001) 701–736.

44. **Bimberg D., Grundmann M., Ledentsov N. N.,** Quantum dot heterostructures, John Wiley & Sons, Chichester, 1999.

45. **Shelawati T., Nurisya M. S., Kar Tim C., Mazliana A. K.,** Effects of step-potential on confinement strength of strain-induced type-I core–shell quantum dots, Superlattices Microstruct. 131 (July) (2019) 95–103.

46. **Guet C., Johnson W. R.,** Dipole excitations of closed-shell alkali-metal clusters, Phys. Rev. B. 45 (19) (1992) 11283–11287.

47. **Ekardt W.,** Size-dependent photoabsorption and photoemission of small metal particles, Phys. Rev. B. 31 (10) (1985) 6360–6370.

48. **Beck D. E.,** Self-consistent calculation of the eigen frequencies for the electronic excitations in small jellium spheres, Phys. Rev. B. 35 (14) (1987) 7325–7333.

49. **Haberland H.** Clusters of atoms and molecules. Theory, experiment, and clusters of atoms (Springer Series in Chemical Physics. Chemical, Vol. 52), Springer, Berlin, Heidelberg, 1994.

50. **De Heer W. A.,** The physics of simple metal clusters: Experimental aspects and simple models, Rev. Mod. Phys. 65 (3) (1993) 611–676.

СПИСОК ЛИТЕРАТУРЫ

1. **Климов В. В.** Наноплазмоника. М.: Физматлит, 2009. 480 с.

2. **Bozhevolniy S. I.**, **Martin-Moreno L., Garcia-Vidal F.** (Eds.) Quantum plasmonics. (Springer Series in Solid-State Sciences. Vol. 185). Cham, Switzerland: Springer International Publishing, 2017. 327 p.

3. **Enoch S., Bonod N.** Plasmonics: From basics to advanced topics. (Springer Series in Optical Sciences. Vol. 167). Heidelberg, Berlin: Springer-Verlag, 2012. 321 p.

4. **Tame M. S., McEnery K. R.,** Özdemir **Ş. K., Lee J., Maier S. A., Kim M. S.** Quantum plasmonics // Nature Physics. 2013. Vol. 9. June. Pp. 329–340.

5. **Scholl J. A., Koh A. L., Dionne J. A.** Quantum plasmon resonances of individual metallic nanoparticles // Nature. 2012. Vol. 483. 22 March. Pp. 421–427.

6. **Brack M.** The physics of simple metal clusters: Self-consistent jellium model and semiclassical approaches // Reviews of Modern Physics. 1993. Vol. 65. No. 3. Pp. 677–732.

7. **Harb M., Rabilloud F., Simon D., Rydlo A., Lecoultre S., Conus F., Rodrigues V., Félix C.** Optical absorption of small silver clusters: Ag_n (n = 4–22) // The Journal of Chemical Physics. 2008. Vol. 129. No. 19. P. 194108.

8. **Xuan F., Guet C.** Core-polarization-corrected random-phase approximation with exchange for dipole surface plasmons in silver clusters // Physical Review A. 2016. Vol. 94. No. 4. P. 043415.

9. **Kreibig U., Vollmer M.** Optical properties of metallic clusters. (Springer Series in Materials Science. Vol. 65). Heidelberg, Berlin: Springer-Verlag, 1995. 535 p.

10. **Kreibig U., Zacharias P.** Surface plasma resonances in small silver and gold particles // Zeitschrift für Physik. 1970. Vol. 231. No. 2. Pp. 128–143.

11. **Kriegel I., Scotognella F., Manna L.** Plasmonic doped semiconductor nanocrystals: Properties, fabrication, applications and perspectives // Physics Reports. 2017. Vol. 674. 28 February. Pp. 1–52.

12. **Klimov V. I.** Nanocrystal quantum dots. Second edition. Boca Raton, Florida, USA: CRC Press, 2010. 485 p.

13. **Monreal R. C., Antosiewicz T. J., Appel S. P.** Competition between surface screening and size quantization for surface plasmons in nanoparticles // New Journal of Physics. 2013. Vol. 15. No. 8. P. 083044.

14. **Scotognella F., Della Valle G., Kandada A. R. S., Zavelani-Rossi M., Longhi S., Lanzani G., Tassone F.** Plasmonics in heavily-doped semiconductor nanocrystals // The European Physical Journal B. 2013. Vol. 86. No. 4. P. 154.

15. **Xie Y., Carbone L., Nobile C., et al.** Metallic-like stoichiometric copper sulfide nanocrystals: Phase- and shape-selective synthesis, near-infrared surface plasmon resonance properties, and their modeling // ACS Nano (The American Chemical Society). 2013. Vol. 7. No. 8. Pp. 7352–7369.

16. **Routzahn A. L., White S. L., Fong L.-K., Jain P. K.** Plasmonics with doped quantum dots // Israel Journal of Chemistry. 2012. Vol. 52. No. 11–12. Pp. 983–991.

17. **Luther J. M., Jain P. K., Ewers T., Alivisators A. P.** Localized surface plasmon resonances arising from free carriers in doped quantum dots // Nature Materials. 2011. Vol. 10. May. Pp. 361–366.

18. **Faucheaux J. A., Stanton A. L. D., Jain P. K.** Plasmon resonances of semiconductor nanocrystals: Physical principles and new opportunities // The Journal of Physical Chemistry Letters. 2014. Vol. 5. No. 6. Pp. 976–985.

19. **Zhang H., Kulkarni V., Prodan E., Nordlander P., Govorov A. O.** Theory of quantum plasmon resonances in doped semiconductor nanocrystals // The Journal of Physical Chemistry. C. 2014. Vol. 118. No. 29. Pp. 16035–16042.

20. **Lounis S. D., Runnerstrom E. L., Bergerud A., Nordlund D., Milloron D. J.** Influence of dopant distribution on the plasmonic properties of indium tin oxide nanocrystals // Journal of the American Chemical Society. 2014. Vol. 136. No. 19. Pp. 7110–7116.

21. **Schimpf A. M., Thakkar N., Gunthardt C. E., Masiello D. J., Gamelin D. R.** Charge-tunable quantum plasmons in colloidal semiconductor nanocrystals // ACS Nano (The American Chemical Society). 2014. Vol. 8. No. 1. Pp. 1065–1072.

22. **Schimpf A. M., Gunthardt C. E., Rinehart J. D., Mayer J. M., Gamelin D. R.** Controlling carrier densities in photochemically reduced colloidal ZnO nanocrystals // Journal of the American Chemical Society. 2013. Vol. 135. No. 44. Pp. 16569–16577.

23. **Liu X., Swihart M. T.** Heavily-doped colloidal semiconductor and metal oxide nanocrystals, an emerging new class of plasmonic nanomaterials // Chemical Society Reviews. 2014. Vol. 43. No. 11. Pp. 3908–3920.

24. **Gerchikov L. G., Guet C., Ipatov A. N.** Multiple plasmons and anharmonic effects in small metallic clusters // Physical Review A. 2002. Vol. 66. No. 5. P. 053202.

25. **Ipatov A. N., Gerchikov L. G., Guet C.** Resonant photoabsorption of metallic clusters in a strong laser field // Computational Materials Science. 2006. Vol. 35. No. 3. Pp. 347–353.

26. **Ipatov A. N., Gerchikov L. G., Guet C.** Plasmon resonance in photoabsorption of colloidal highly doped ZnO nanocrystals // Nanoscale Research Letters. 2018. Vol. 13. No. 1. P. 297.

27. **Ипатов А. Н., Герчиков Л. Г.** Вращательная дипольная плазмонная мода в наноразмерных полупроводниковых частицах // Журнал экспериментальной и теоретической физики. 2021. Т. 159. № 6. С. 1047–1069.

28. **Yabana K., Bertsch G. F.** Electronic structure of C_{60} in a spherical basis // Physica Scripta. 1993. Vol. 48. No. 5. Pp. 633 –637.

29. **Ju N., Bulgac A., Keller J. W.** Excitation of collective plasmon states in fullerenes // Physical Review B. 1993. Vol. 48. No. 12. Pp. 9071–9079.

30. **Ostling P., Apell P., Rosén A.** Theory for collective resonances of the C_{60} molecule // Europhysics Letters. 1993. Vol. 21. No. 5. Pp. 539–544.

31. **Madjet M., Guet G., Johnson W. R.** Comparative study of exchange-correlation effects on electron and optical properties of alkali-metal clusters // Physical Review A. 1995. Vol. 51. No. 2. Pp. 1327–1339.

32. **Mukherjee D.** Applied many-body methods in spectroscopy and electronic structure. New York, USA: Springer, 1992. 299 p.

33. **Serra Ll., Garcias F., Navarro J., Barberán N., Barranco M., Pi M.** Electronic surface excitations of cavities in metals // Physical Review B. 1992. Vol. 46. No. 15. Pp. 9369–9379.

34. **Варшалович Д. А., Москалев А. Н., Херсонский В. К.** Квантовая теория углового момента. Ленинград: Наука, 1975. 439 с.

35. **Ipatov A. N., Gerchikov L. G.** Many-particle correlations in microscopic electron-hole droplets // Journal of Physics B: Atomic, Molecular and Optical Physics. 2014. Vol. 47. No. 18. P. 185101.

36. **Герчиков Л. Г., Ипатов А. Н.** Коллективные возбуждения в оптических спектрах наноразмерных экситонных и электрон-позитронных капель // Журнал экспериментальной и теоретической физики. 2014. Т. 5 № .146. С. 1025–1014.

37. **Амусья М. Я., Чернышева Л. Я.,** Яржемский **В. Г.** Поглощение фотонов, рассеяние электронов, распад вакансий. Атомные данные. СПб.: Наука, 2010. 314 с.

38. **Dreizler R. M., Gross E. K. U.** Density functional theory: An approach to the quantum many-body problem. Berlin: Springer, 1990. 302 p.

39. **Ландау Л. Д., Лифшиц Е. М.** Теоретическая физика. В 10 тт. Т. 3. Квантовая механика (нерелятивистская теория). -4е изд., испр. М.; Наука. Гл. ред. физ.-мат. лит-ры, 1989. 768 с.

40. **Ипатов А. Н., Герчиков Л. Г.** Стабильность и свойства конечных Ферми-систем, содержащих частицы разной массы // Журнал экспериментальной и теоретической физики. 2014. Т. 1 № .145. С. 119–108.

41. **Собельман И. И.** Введение в теорию атомных спектров. М.: Наука. Главная редакция физ.-мат. лит-ры, 1977. 320 с.

42. **Banin U., Cao Y., Katz D., Millo O.** Identication of atomic-like electronic states in indium arsenide nanocrystal quantum dots // Nature. 1999. Vol. 400. 5 August. Pp. 542–544.

43. **Kouwenhoven L. P., Austing D. G., Tarucha S.** Few electron quantum dots// Reports on Progress in Physics. 2001. Vol. 64. No. 6. Pp. 701–736.

44. **Bimberg D., Grundmann M., Ledentsov N. N.** Quantum dot heterostructures. Chichester: John Wiley & Sons, 1999. 338 p.

45. **Shelawati T., Nurisya M. S., Kar Tim C., Mazliana A. K.** Effects of step-potential on confinement strength of strain-induced type-I core—shell quantum dots // Superlattices and Microstructures. 2019. Vol. 131. July. Pp. 95—103.

46. **Guet C., Johnson W. R.** Dipole excitations of closed-shell alkali-metal clusters // Physical Review B. 1992. Vol. 45. No. 19. Pp. 11283—11287.

47. **Ekardt W.** Size-dependent photoabsorption and photoemission of small metal particles // Physical Review B. 1985. Vol. 31. No. 10. Pp. 6360—6370.

48. **Beck D. E.** Self-consistent calculation of the eigen frequencies for the electronic excitations in small jellium spheres // Physical Review B. 1987. Vol. 35. No. 14. Pp. 7325—7333.

49. **Haberland H.** Clusters of atoms and molecules. Theory, experiment, and clusters of atoms (Springer Series in Chemical Physics. Chemical, Vol. 52), Berlin, Heidelberg: Springer, 1994. 422 p.

50. **De Heer W. A.** The physics of simple metal clusters: Experimental aspects and simple models // Reviews of Modern Physics. 1993. Vol. 65. No. 3. Pp. 611—676.

THE AUTHORS

IPATOV Andrei N.
Peter the Great St. Petersburg Polytechnic University;
Alferov University of RAS
29 Politechnicheskaya St., St. Petersburg, 195251, Russia
andrei_ipatov@mail.ru

KUPRIIANOV Genrikh A.
Peter the Great St. Petersburg Polytechnic University
29 Politechnicheskaya St., St. Petersburg, 195251, Russia
henryweis3@gmail.com

СВЕДЕНИЯ ОБ АВТОРАХ

ИПАТОВ Андрей Николаевич – *доктор физико-математических наук, профессор кафедры физики Санкт-Петербургского политехнического университета Петра Великого и профессор кафедры физики и технологии наногетероструктур Санкт-Петербургского академического университета им. Ж. И. Алфёрова РАН.*
195251, Россия, г. Санкт-Петербург, Политехническая ул., 29
andrei_ipatov@mail.ru

КУПРИЯНОВ Генрих Александрович – *ассистент кафедры физики Санкт-Петербургского политехнического университета Петра Великого.*
195251, Россия, г. Санкт-Петербург, Политехническая ул., 29
henryweis3@gmail.com

Received 31.03.2023. Approved after reviewing 21.04.2023. Accepted 21.04.2023.
Статья поступила в редакцию 31.03.2023. Одобрена после рецензирования 21.04.2023. Принята 21.04.2023.